Evaluation of Various Numerical Methods in LS-DYNA® for 3D Crack Propagation

Ala Tabiei and Wenlong Zhang
Department of Mechanical Engineering
University of Cincinnati, Cincinnati, OH 45221-0070

Abstract

In this paper, four different numerical methods implemented in the large scale simulation code LS-DYNA® are evaluated to determine their abilities and limitations in fracture problems especially 3-d crack propagation problems. These methods are: Finite Element Method (FEM), Discrete Element Method (DEM), Element Free Galerkin (EFG) method and Extended Finite Element Method (XFEM). Their methodologies are briefly described and several numerical simulations are carried out and compared with experiment results. In some examples, fracture parameters are evaluated and mesh sensitivity is studied. Their potentials and limitations are discussed.

Keywords*: Crack propagation; Discrete element method; Finite element method; Element free Galerkin method; Extended finite element method; LS-DYNA*

Introduction

Finite element method (FEM) has been a powerful tool for modeling crack initiation, propagation and calculating fracture parameters. Contributions are continuously made to finite element method in the past few decades to improve its ability to handle complicated fracture problems. Meanwhile new methodologies have been proposed to deal with issues that standard FEM is hard to deal with. The ability of four different methods in LS-DYNA are evaluated in this paper:

a) The Finite Element Method (FEM)
b) The Discrete Element Method (DEM)
c) The Element-Free Galerkin method (EFG)
d) The Extended Finite Element Method (XFEM)

Their methodologies are briefly explained and several simulations are carried out and compared to experiment results.

Finite Element Method

Three basic methods can be used in finite element code to simulate crack growth, including smeared crack approach, nodal release approach and delete-and-fill remeshing approach. A summary that describes these three methods can be found in [1]. In this study, fracture models were implemented in the DYNA3D code for 3-D crack growth simulations. The implemented fracture models have the capabilities of simulating automatic crack propagation in solid elements without user intervention. Fracture parameters are evaluated and various crack growth criteria are implemented.

Evaluation of Fracture Parameters

In the finite element code DYNA3D, a 3-D crack is modeled with edges and surfaces of solid elements by a series of "sub-cracks" at the crack front (Fig. 1). Each sub-crack is defined by three nodes with the identification numbers 1, 2 and 3. For through thickness crack, the fracture parameters are taken as the average of the results obtained from all the sub-cracks it encompasses. The evaluated fracture parameters in this procedure include the stress intensity factors (K_I, K_{II}, K_{III}), energy release rates (G_I, G_{II}, G_{III}), and crack tip opening angle (CTOA).

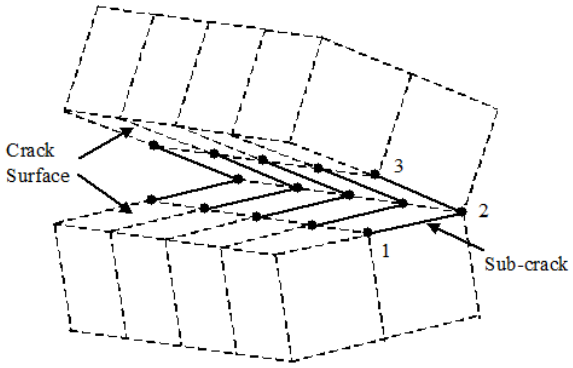

Figure 1. Decomposition of a 3-D crack tip. [1]

Stress intensity factors (SIFs) of the three fracture modes (see Fig. 2) are extracted at discrete nodes from the elastic solution [2] of a cracked geometry:

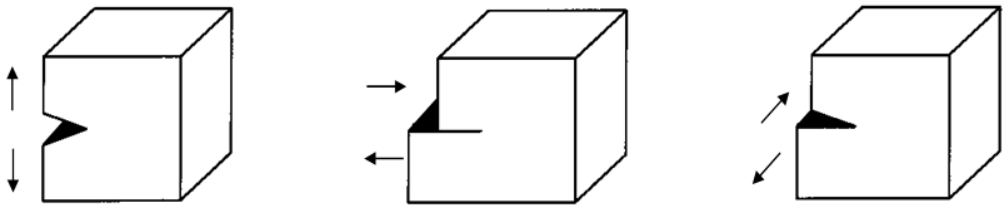

(a) Mode I (*opening mode*) (b) Mode II (*shearing mode*) (c) Mode III (*tearing mode*)

Figure 2. Three modes of fracture

$$K_I = \frac{E}{(1+\nu)(1+\kappa)}\sqrt{\frac{\pi}{2r}}\left(x_{b_{node3}} - x_{b_{node1}}\right) \quad (1)$$

$$K_{II} = \frac{E}{(1+\nu)(1+\kappa)}\sqrt{\frac{\pi}{2r}}\left(x_{n_{node3}} - x_{n_{node1}}\right) \quad (2)$$

$$K_{III} = \frac{E}{4(1+\nu)}\sqrt{\frac{\pi}{2r}}\left(x_{t_{node3}} - x_{t_{node1}}\right) \quad (3)$$

Where E is the Young's modulus; ν is the Poisson's ratio; and κ is the Kolosov constant defined as

$$\kappa = \begin{cases} 3 - 4\nu, & plane\ strain \\ \dfrac{3-\nu}{1+\nu}, & plane\ stress \end{cases} \tag{4}$$

The total energy release rate, G, is the amount of energy released at the crack tip per unit area for the crack extension process. The expression is given as [3,3,3]:

$$G = -\frac{\partial \Pi}{\partial a} = -\frac{\partial (U - W)}{\partial a} = G_I + G_{II} + G_{III} \tag{5}$$

Where Π is the total potential energy per unit thickness; U is the strain energy of the structure per unit thickness; W is the work of the external tractions per unit thickness, and a is the crack length. The energy release rates are directly calculated from the stress intensity factors using the following relationships [4]:

$$G_i = \frac{1}{E'} K_i^2 \; i = 1,2,3 \tag{6}$$

Where E is Young's modulus, ν is Poisson's ratio, and $E' = E$ (plane stress) or $E' = E/(1 - \nu^2)$ (plane strain).

For crack tip opening angle, it is evaluated based on sub-crack angles. In the simulation of uniform crack growth, the actual 3-D crack angle is considered as the average of all the sub-crack angles.

Implementation of the 3-D Crack Growth Criteria

Where E is the Young's modulus; ν is the Poisson's ratio; and κ is the Kolosov constant defined as

$$\kappa = \begin{cases} 3 - 4\nu, & plane\ strain \\ \dfrac{3-\nu}{1+\nu}, & plane\ stress \end{cases} \tag{7}$$

The total energy release rate, G, is the amount of energy released at the crack tip per unit area for the crack extension process. The expression is given as [3,3,3]:

$$G = -\frac{\partial \Pi}{\partial a} = -\frac{\partial (U - W)}{\partial a} = G_I + G_{II} + G_{III} \tag{8}$$

Where Π is the total potential energy per unit thickness; U is the strain energy of the structure per unit thickness; W is the work of the external tractions per unit thickness, and a is the crack length. The energy release rates are directly calculated from the stress intensity factors using the following relationships [4]:

$$G_i = \frac{1}{E'} K_i^2 \; i = 1,2,3 \tag{9}$$

Where E is Young's modulus, ν is Poisson's ratio, and $E' = E$ (plane stress) or $E' = E/(1 - \nu^2)$ (plane strain).

For crack tip opening angle, it is evaluated based on sub-crack angles. In the simulation of uniform crack growth, the actual 3-D crack angle is considered as the average of all the sub-crack angles.

Implementation of the 3-D Crack Growth Criteria

Several crack growth criteria have been implemented in the nonlinear explicit finite element code DYNA3D. These crack growth criteria include maximum principal stress based criterion, CTOA based crack growth criterion [5,6], SIFs-based criterion [7], and energy release rate based criterion [8]. The crack growth direction is predicted using formula proposed by [9]:

$$\theta_0 = 2tan^{-1}\left(\frac{-2K_{II}}{K_{leff} + \sqrt{\left(K_{leff}\right)^2 + 8(K_{II})^2}}\right) \tag{10}$$

Discrete Element Method

The Discrete Element Method (DEM) was proposed by Cundall (1979) [10] as a numerical method to describe the mechanical behavior of assemblies and discs, and each element is represented by a node at the element center. Interactions such as spring, damper and friction are built between discrete elements, and such assembly of microstructures will give it emergent macro properties like elastic modulus, material toughness and so on [11].

Recently DEM's application on fracture simulation in dense materials is gaining popularity. Unlike FEM, DEM treats fracture as discrete approach: a successive break of bonds between particles, which allows for natural and realistic crack propagation [12]. Various criteria are available to predict the bond break.

A simple criterion is maximum normal or shear force criterion [13-17]. When the normal and shear bond force reaches the rupture threshold, they will drop to zero and the bond fails. Fracture toughness K_{IC} and critical energy release rate G_{IC} based criteria were also developed [18]. Strain energy density (SED) criterion first proposed by Sih (1974) [5] is used in LS-DYNA. It works in a way that fracture happens when the strain energy density (S) reaches a critical value (S_c). The total critical strain energy density is taken as the gross area of the stress strain curve from uniaxial tensile test. S_v and S_d are calculated using equation (8~10) [19].

$$S_v = \frac{1-v}{6E}(\sigma_1 + \sigma_2 + \sigma_3)^2 \tag{11}$$

$$S_d = \frac{1+v}{6E}[(\sigma_1 - \sigma_2)^2 + (\sigma_2 - \sigma_3)^2 + (\sigma_3 - \sigma_1)^2 + 6(\tau_{12}^2 + \tau_{23}^2 + \tau_{13}^2)] \tag{12}$$

$$S = S_v + S_d \tag{13}$$

Minimum time step for discrete element method

Discrete element method is an explicit method so minimum time step is required to ensure that there is no penetration of the particles, otherwise the velocity of spheres will be too large to keep the system stable. A minimum time step used LS-DYNA is calculated based on the Cundall approach [20]:

$$dt = 0.2\pi \sqrt{\frac{\rho(4/3)\pi {r_{sphere}}^2}{\frac{E}{[3(1+2v]} NormK}} \tag{14}$$

Where NormK is a stiffness penalty parameter defined in *control_discrete_element.

Element Free Galerkin Method

The Element Free Galerkin (EFG) method was developed by T. Belytschko [21]. He used the moving least square (MLS) interpolant and weight function to construct discrete system function in variation form. A detailed explanation about continuous or discrete MLS approximation can be found in [22]. In EFG method no element is needed since only a mesh of nodes and boundary condition is used to develop the Galerkin form. This gives it advantages when it comes to crack propagation problems: EFG method doesn't need to remesh because crack growth is simply modeled by extending free surfaces [23].

In the past two decades, large amount of developments is made to EFG methods. In 1995, T. Belytschko developed a coupled finite element-mesh free Galerkin method and obtained consistency and continuity at the interface between two methods [24]. This makes it possible to apply EFG method to only the fracture region while use finite element method in other regions, because the computation cost for EFG is higher than FEM. In 2001, P.A Klein et al developed the general formulation of the nodal force vector and tangent stiffness matrix for cohesive surface elements and apply these formulations to mesh-free representation of displacement field [RW.ERROR - Unable to find reference:211]. In LS-DYNA EFG method is used in combination with cohesive zone model [25]. MAT_185 Tvergaard and Hutchinson model [26] is used. This cohesive model defines a trapezoidal traction-separation law, as shown in Fig 3. Detailed information about formulation of this cohesive model can be found in LS-DYNA material manual *MAT185.

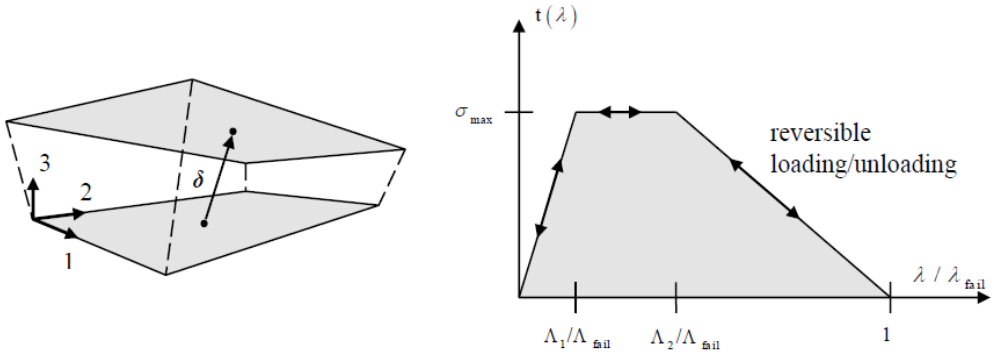

Figure 3: LS-DYNA *mat_185 cohesive material traction-separation law

Extended Finite Element Method

Extended finite element method (XFEM) was developed to handle the discontinuity, singularity and high gradients field in standard finite element method (FEM) [27]. The basic idea of XFEM

is to add some enrichment functions to FEM's polynomial space to handle the non-smooth properties so that minimum re-meshing is needed throughout the simulation. The enrichment function uses a concept of partition of unity (PU) [28,29]. A detailed description of PU concept can be found in [30,31]. Level set method is used to find open or closed interface in XFEM [32]. Consider a d-dimensional domain $\Omega \in \mathbb{R}^d$, which is discretized by n^{el} elements, numbered from 1 to n^{el}. I is the set of all nodes in the domain, and I_k^{el} is the nodes of element k. $I^* \subset I$ is where discontinuity happens. A standard XFEM approximation has a form [33] :

$$\boldsymbol{u}^h(\boldsymbol{x}) = \sum_{i \in I} N_i(x) u_i + \sum_{i \in I^*} N_i^*(x)[\psi(x) - \psi(x_i)]a_i \tag{15}$$

The second term in equation is the enrichment added to the FE formulation and $\psi(x)$ is called enrichment function, a_i is additional nodal unknown. Equation 12 has Kronecker- δ property and its value becomes the same as FE formulation at nodes. A common choice of enrichment function is generalized Heaviside function [34]. Details about crack enrichment can be found in [28,35].

The implementation of XFEM into LS-DYNA code is described by [25]. It is also used in combination with cohesive zone model by Tvergaard [RW.ERROR - Unable to find reference:285].

Numerical Simulations

Steel specimen under tension

A steel specimen under tension is simulated using FEM, DEM, EFG and XFEM in LS-DYNA. Fig. 4 and Table 1 shows the dimension of the specimen in accordance with ASTM E8 standard [36] with a unit mm. The simulation is displacement controlled and a constant velocity ($5mm/ms$) is applied the right end of specimen while the left end is fixed.

AISC 4340 steel with elastic modulus $201\,Gpa$ and yield stress $710\,Mpa$ is used. Material model *MAT_PLASTIC_KINEMATIC is used to define the yielding point and give it a plastic behavior.

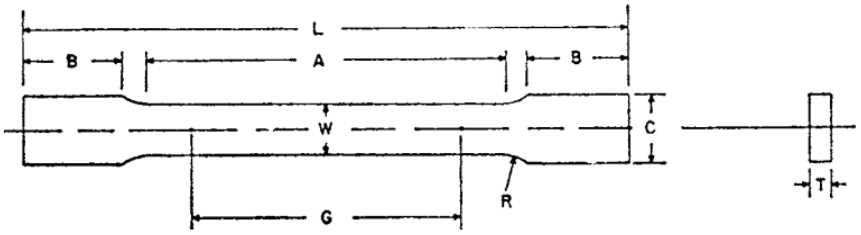

Figure 4. AISC 4340 steel tension specimen size illustration (ASTM E8 standard)

Table.1 AISC 4340 steel tension specimen size specification

Symbol	W	T	R	L	A	B	C
Value (mm)	12.5	2.64	12.5	200	60	50	20

The simulation using discrete element method is carried out using multiple mesh sizes and different nodes arrangements to see mesh sensitivity and influence of element arrangement (Table.2). The Stress strain curves are obtained and the regular coarse mesh result is compared with FEM, EFG and XFEM result.

Table.2 Description of different DEM test groups

Element arrangement	Number of Elements
Regular	3800
Regular	30000
Random	30000

From Fig. 5 we can see the crack appears at the same location for cases with regular and random element spacing. When regular element arrangement is used, there is element exploding when fracture happens. Mesh sensitivity is observed in DEM although not obvious (Fig. 6(a)). Results from FEM, EFG, XFEM and DEM are close (Fig.6 (b)).

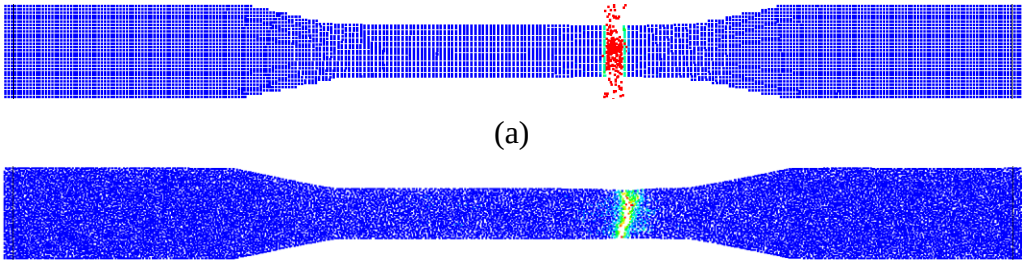

(a)

(b)

Figure 5: Crack in discrete element model (a) regularly arranged elements (b) Randomly arranged elements

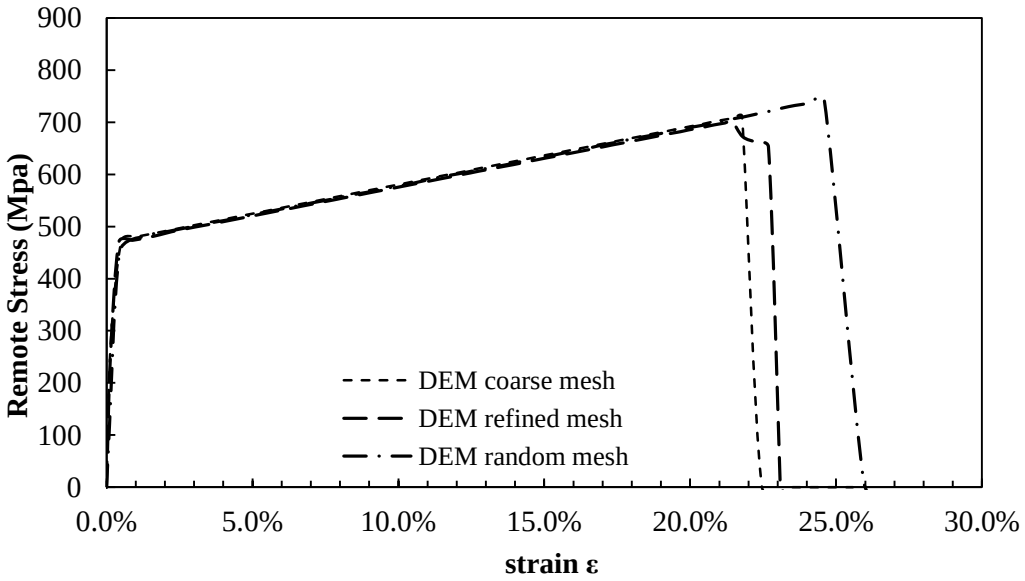

Figure 6: (a) Mesh sensitiviy study for Discrete Element Method

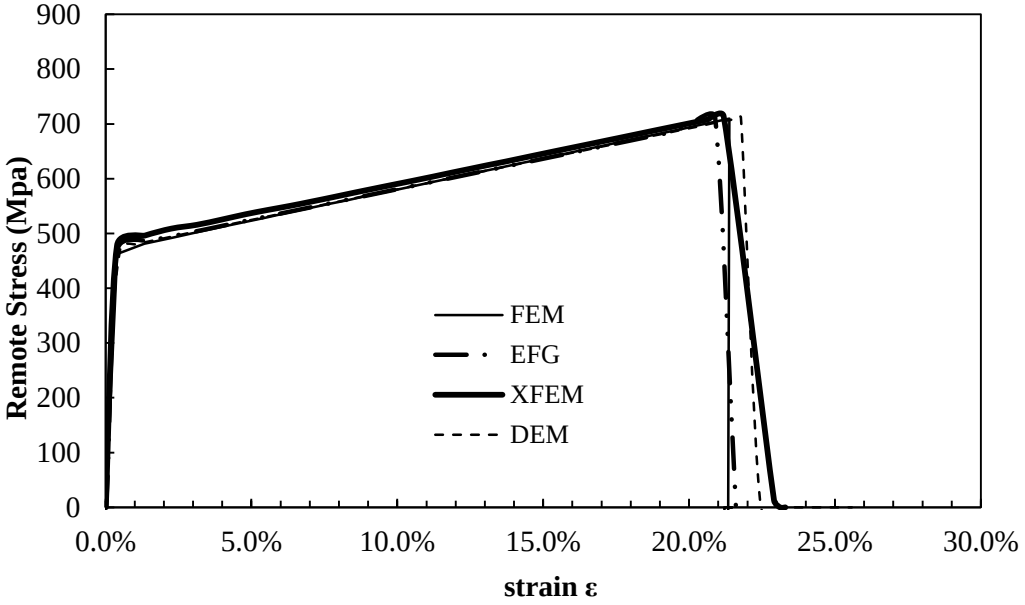

Figure 6: (b) Stress-strain curve of different methods

Crack growth of Aluminum 2024-T3 plate under uniaxial tension

Gullerud et al. (1999) [6] presented the load-crack extension experimental data from five 2024-T3 M(T) aluminum specimens tested at NASA-Langley. A tensile load is incrementally applied to the plate by displacement control and the load versus crack extension curve is measured. Opposite constant velocities (*V*) are imposed on both ends of the plate. The loading rate (V/L_0) is taken as $0.25s^{-1}$. All the four methods are used to verify the crack propagation vs. remote stress curve (Fig. 7).

The material properties of 2024-T3 aluminum alloy used here is provided by [37]: an elastic modulus of $71400\ MPa$ and a yield stress of $345\ MPa$.

The CTOA criterion is employed to predict the crack growth in FEM. The critical CTOA value is taken as 5.25° [37]. In discrete element model, only regular arrangement of elements is used to measure the crack length as it's hard to determine crack tip location in a random arrangement model.

For EFG and XFEM, the critical energy release rate $G_{IC} = 9.47MPa \cdot mm$ is used for cohesive model. The load-crack extension curve for these three methods are plotted and compared with experimental results (Fig. 8).

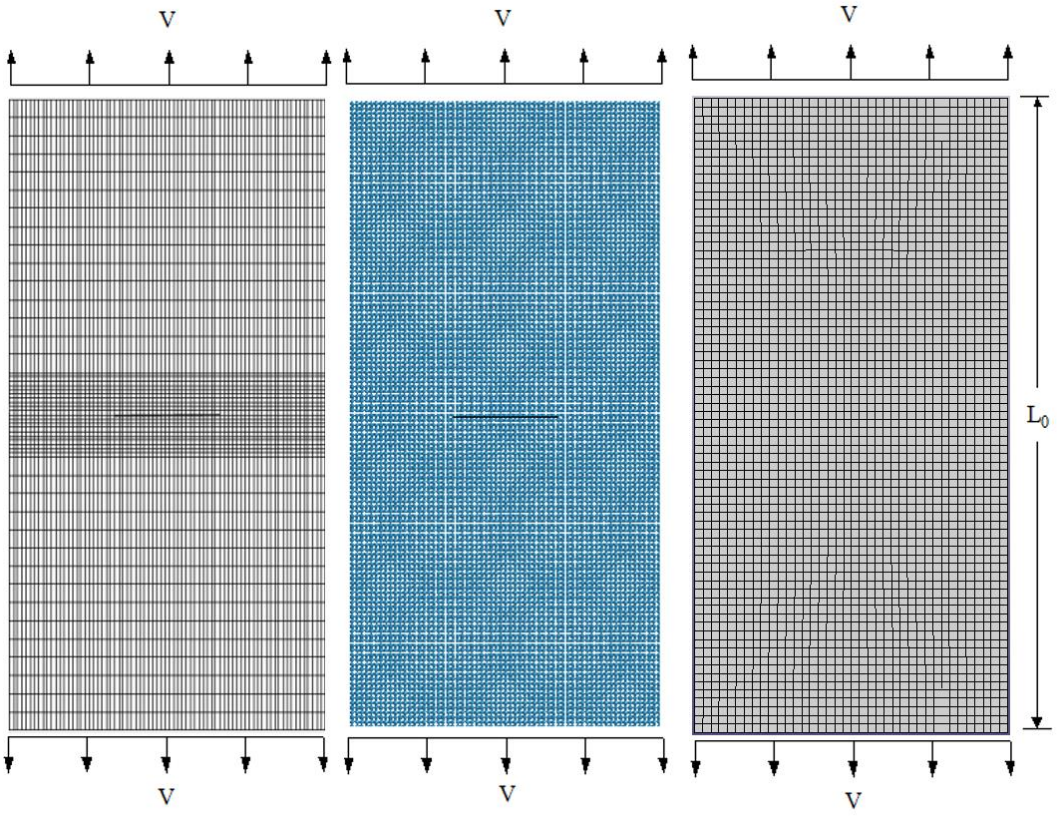

Figure 7: Finite element (left) discrete element (middle) and XFEM (right) model of Alumimum plate

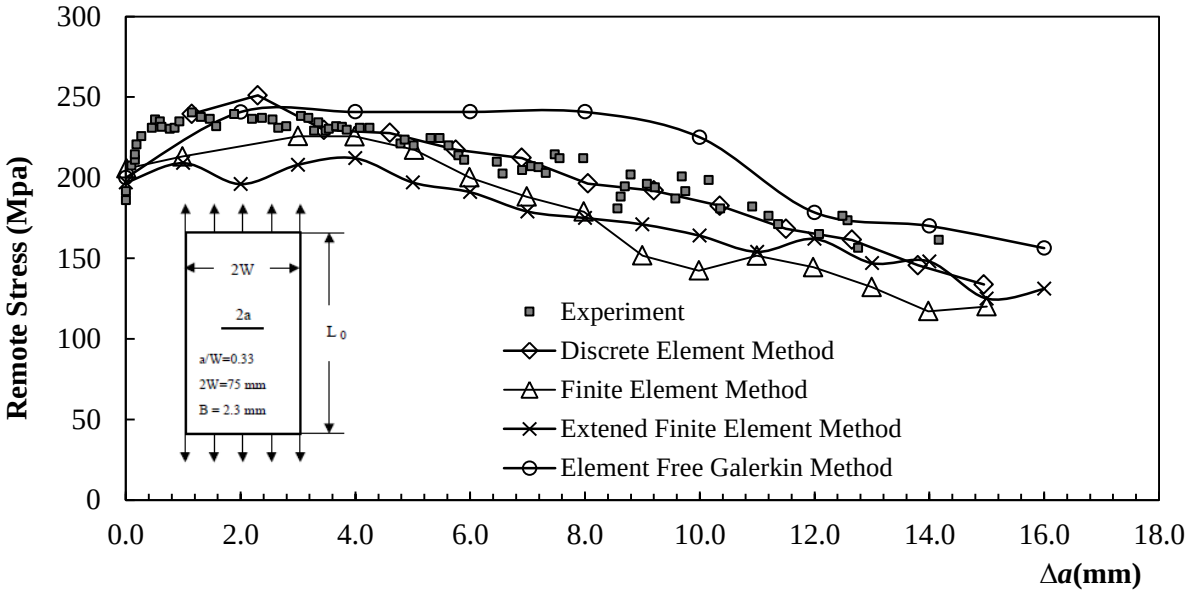

Figure 8: Comparison of experimental and analytical load-crack growth response

Mixed-mode fracture of a central horizontal crack in a square plate

A square plate with a central horizontal crack [38] is simulated (Fig. 9). The plate is subjected to mixed-mode loading of a normal stress σ_y (mode I) and shear stress τ_{xy} (mode II). Eight cases with different stress ratios are considered in this example (Table 3). Linear elastic properties are used: E = 210000 MPa, v = 0.28. The CTOA criterion is employed in the FEM model to activate crack advancement. The critical value is taken as 0.19. XFEM model is also created to compare the results.

For an infinite plate with central crack under mixed-mode loading as shown in Fig. 9, the stress intensity factors (K_I and K_{II}) can be expressed in terms of the normal and shear stresses as follows [39]:

$$K_I = \sigma_y\sqrt{\pi a} = s\sigma\sqrt{\pi a} \tag{16}$$

$$K_{II} = -\tau_{xy}\sqrt{\pi a} = -t\sigma\sqrt{\pi a} \tag{17}$$

Substituting K_I and K_{II} into equation (7) leads to the crack growth angle θ_0 prediction equation as follows:

$$\theta_0 = 2tan^{-1}\left(-\frac{s}{4t}+\frac{1}{4}\sqrt{\left(\frac{s}{t}\right)^2+8}\right) \tag{18}$$

Equation (15) is used here to compute the theoretical crack growth with the different ratios (s/t) of stress factors. The theoretical and simulated results are listed in Table 3 for comparison.

Table 3. Crack growth angle under mixed-mode loading

Case	s	t	θ(Theoretical)	θ(FEM)	θ(XFEM)
1	1	0.1	11.203°	11.375°	11.041°
2	1	0.2	21.089°	21.401°	19.983°
3	1	0.3	29.103°	29.623°	29.106°
4	1	0.4	35.357°	35.898°	34.493°
5	1	0.5	40.208°	40.607°	39.555°
6	1	0.6	44.004°	44.243°	43.958°
7	1	0.7	47.022°	47.918°	47.822°
8	1	0.8	49.460°	49.068°	48.821°

From table 3 we can see that the current implementation of the fracture model predicted the mix-mode crack growth direction very well.

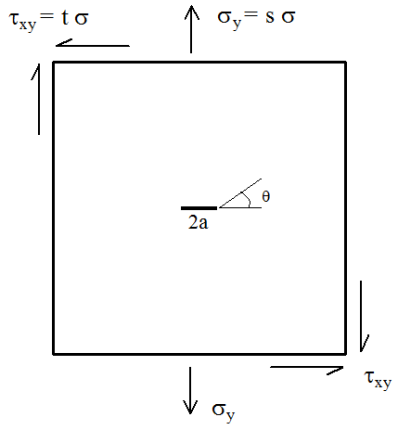

Figure 9: Plate with central horizontal crack under mixed-mode loading

Mode one stress intensity factor

SIF is evaluated using different methods in this section. To obtain the "static" K_I, the traction is applied as a ramp load first and then kept constant after 1.0 millisecond for total of 2.0 milliseconds simulation (Fig. 10).

The specimen used in this model is a rectangular steel plate with a central crack. The specimen size is $8mm \times 16mm \times 1mm$, and the crack length is $4mm$. A traction $\sigma = 200\,MPa$ is applied to both ends. The theoretical value of stress intensity factors can be found in [40]:

$$K_I = \sigma\sqrt{\pi a}F(a/b) \tag{19}$$

For $a/b = 0.5$, $F(a/b) = 1.1864$. When $\sigma = 200$, $K_I = 200 \times \sqrt{2\pi} = 593Mpa\sqrt{mm}$

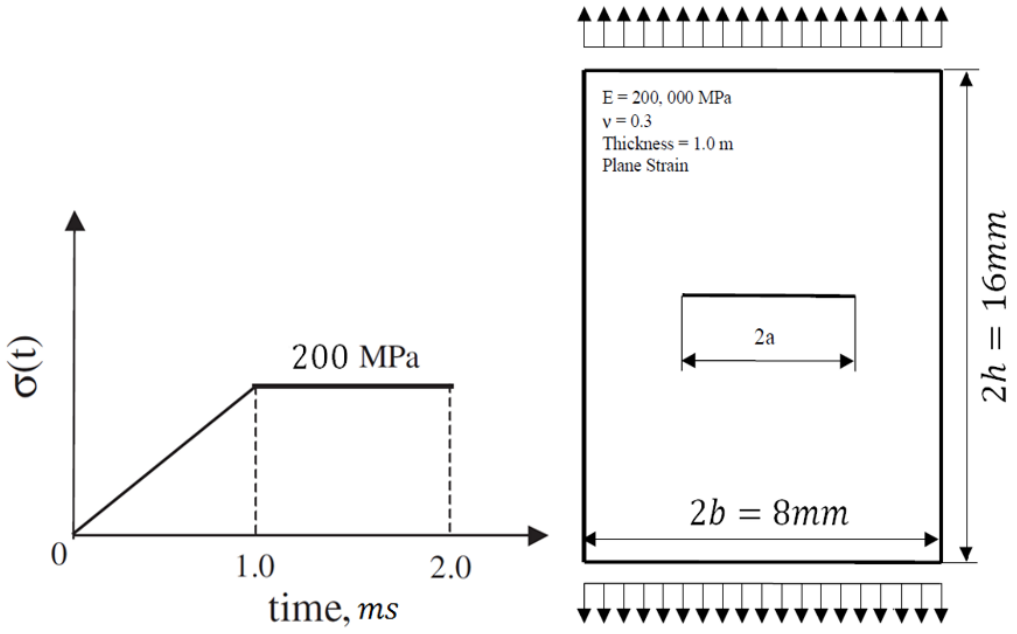

Figure 10: Loading and specimen

Numerical value of SIF is calculated using equation (1~3). Mesh size is small enough so the numerical error is negligible. Relative error between numerical and theoretical value is calculated and tabulated in Table 4. EFG method gives smaller SIF value than theoretical, and there is 11.63% difference. All other methods give good result.

Table 4. Stress intensity value calculated using different methods

	SIF	Relative Error
FEM	576.77	2.70%
DEM	601.05	1.40%
EFG	523.85	11.63%
XFEM	576.00	2.72%

Crack propagation in vitreous biopolymer material

Crack propagation in a biopolymer plate under tensile load is simulated in this section (Fig. 11). This experiment was done by [15] and simulated in LS-DYNA using DEM and XFEM. In DEM, discrete elements are arranged regularly and randomly to show the influence of element arrangement type on the crack path. Their crack shapes are compared to those in the experiment and theoretical values.

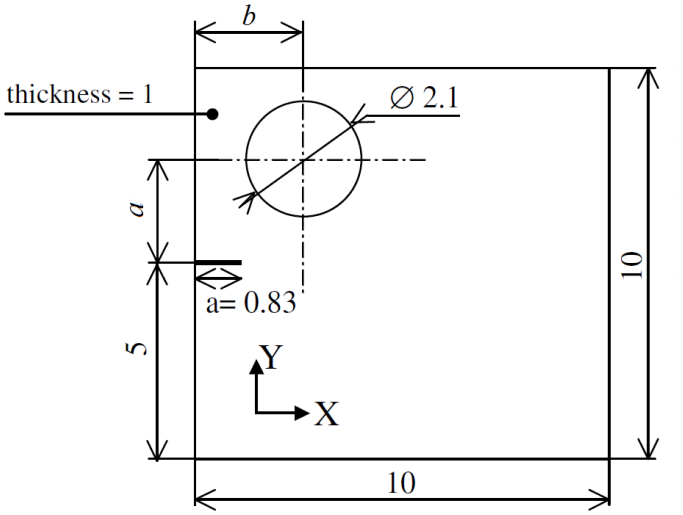

Figure 11: Size of biopolymer plate [41]

Three groups of specimen are crafted and center of hole is at different coordinates (a, b) for different groups:

- Case A: $(3.34,3.30)mm$
- Case B: $(1.83,2.78)mm$
- Case C: $(0.60, 3.05)\ mm$

The experiment is displacement controlled at a rate of 40μm/s. Material properties are taken from paper [15]. Elastic modulus is $E = 0.312Gpa$, Poisson's ratio is $v = 0.3$and $\rho = 1.209g/mm^3$ [42]. The mode 1 fracture toughness is $K_{Ic} = 0.49Mpa\sqrt{m}$ from paper [41].
Two ways of comparison are provided: image analysis [41] and theoretical crack deflection function [43]. The theoretical equation for crack path is given in equation (17) and (18). The a, b, r values are illustrated in Fig. 12

$$y(x) = \frac{r^2}{2b}[2 - t(2 + t - t^2)] \tag{20}$$

$$t = \frac{b - x}{\sqrt{b^2 + (a - x^2)}} \tag{21}$$

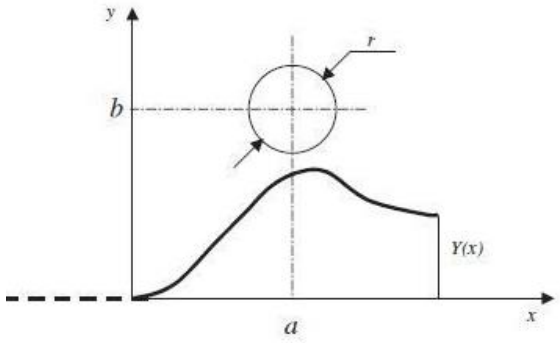

Figure 12: Theoretical crack shape in specimen

Crack path shape for threes cases are shown in figure 13~15. For case b, both DEM and XFEM show a crack path that passes the hole, which is not the case in experiment and theoretical crack path. For case a and c, both methods show similar path shape to experiment and show crack branching. However, when the elements are regularly arranged in discrete element model, it's not able to capture the crack direction and crack branching (Fig. 16).

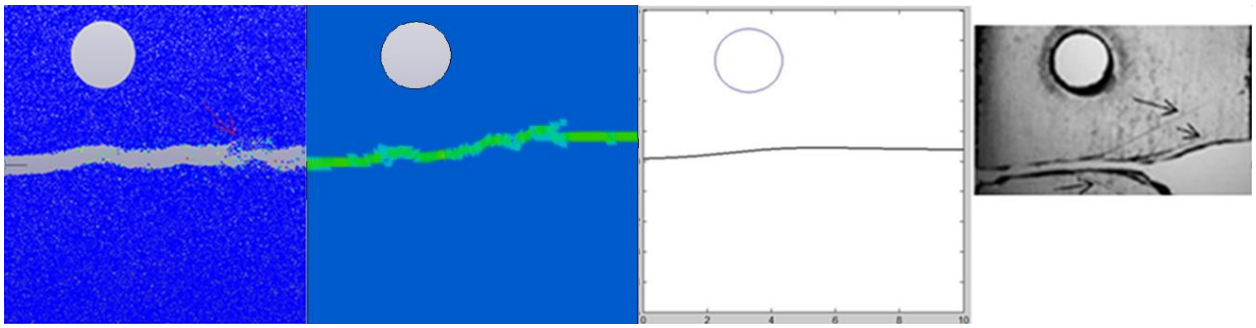

(a) (b) (c) (d)

Figure 13: Case A (a) DEM (b) XFEM (c) Theoretical crack path (d) Crack path from [15]

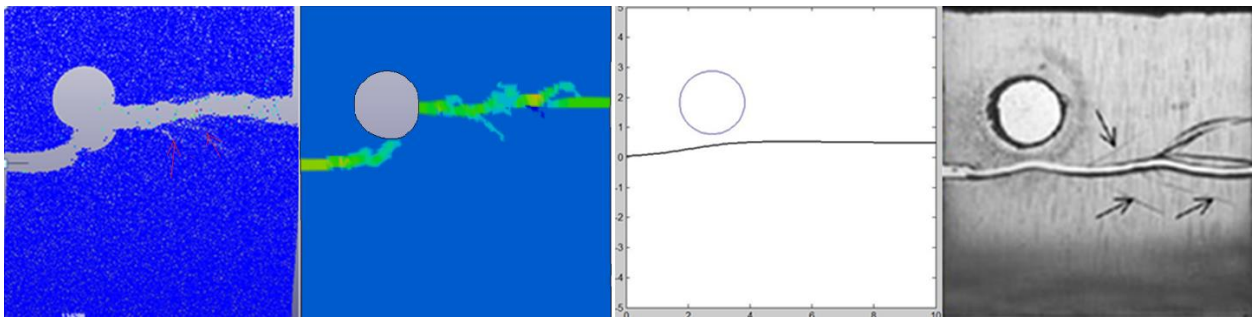

(a) (b) (c) (d)

Figure 14: Case A (a) DEM (b) XFEM (c) Theoretical crack path (d) Crack path from [15]

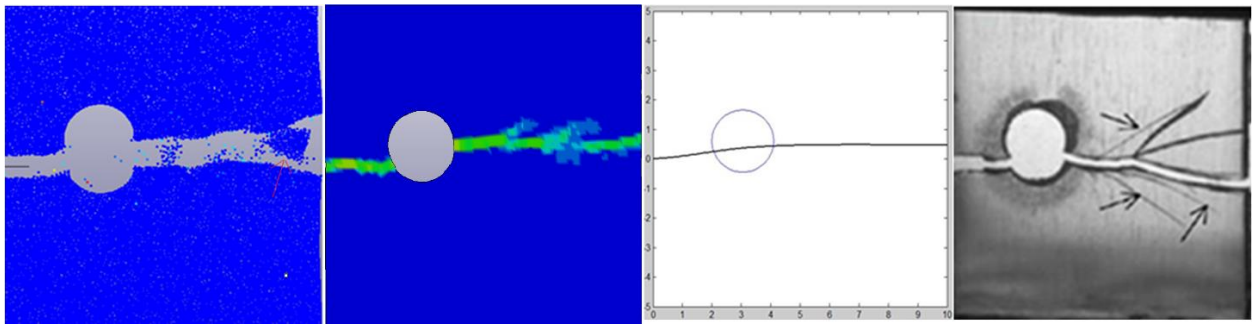

(a) (b) (c) (d)

Figure 15: Case A (a) DEM (b) XFEM (c) Theoretical crack path (d) Crack path from [15]

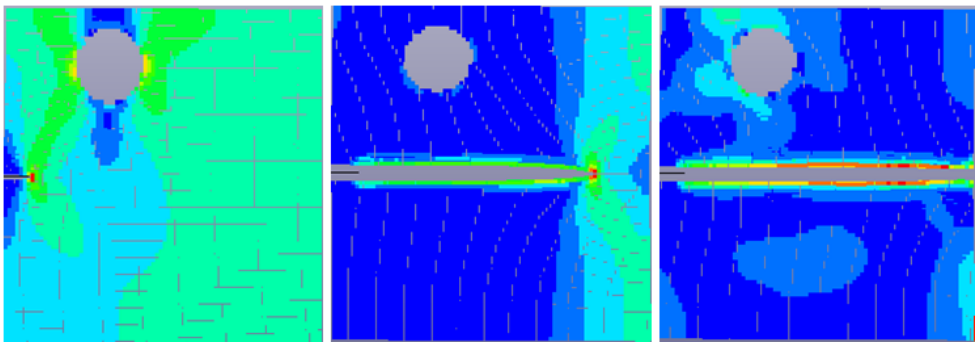

Figure 16: Crack path in regular discrete element arrangement

Crack propagation analysis of rock like Brazilian disc

In this simulation, a rock disc with a pre-crack compressed by a line load is modeled. There is a pre-crack in the disc center with a length of $2b = 10mm$, and arranged with an angle φ from y axis. Four different tests are done and φ is taken as $0^{\circ}, 30^{\circ}, 60^{\circ}, 90^{\circ}$ respectively for each test. Disc specimens have a radius of $42mm$ and thickness of $25mm$ (Fig. 17). Experimental test is done by Hadi [44]. The specimens are loaded till failure and different crack shapes can recorded.

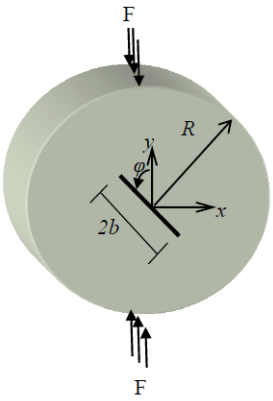

Figure 17: Rock disc specimen with initial crack [44]

Material properties used here are [44]: $E = 15Gpa$, $v = 0.21$, tensile strength $\sigma_t = 3.81Mpa$, and fracture toughness $K_{IC} = 2\,MPa \cdot m^{1/2}$. Simulation is done using EFG method, the maximum load during the test is $16KN$, which agrees well with the experiment result. Comparison between simulation and result crack paths are shown in figure 18~21. The crack shape looks similar but the element deletion method makes it hard to visualize as more elements are deleted.

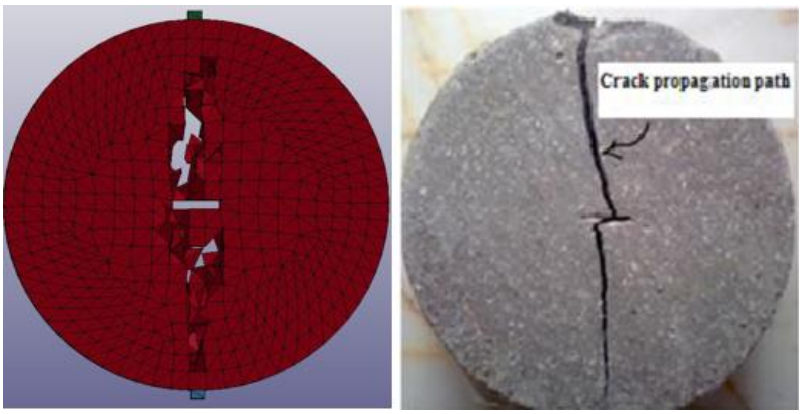

(a) Crack propagation path in EFG result (b) Experiment result [44]

Figure 18: Crack shape when $\varphi = 90^{\circ}$

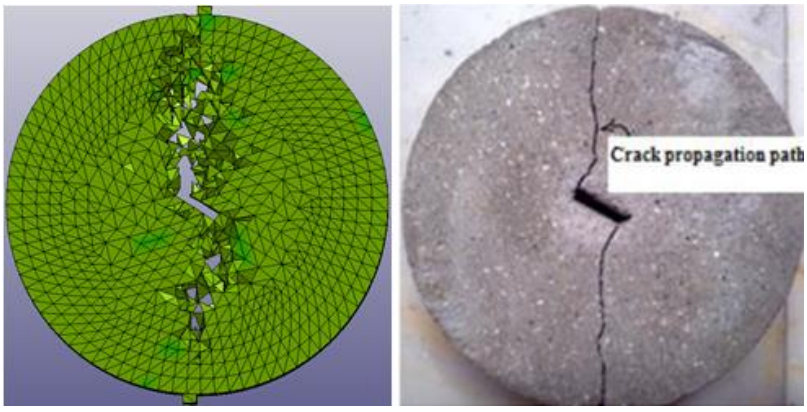

(a) Crack propagation path in EFG result (b) Experiment result [44]

Figure 19: Crack shape when $\varphi = 60^{\circ}$

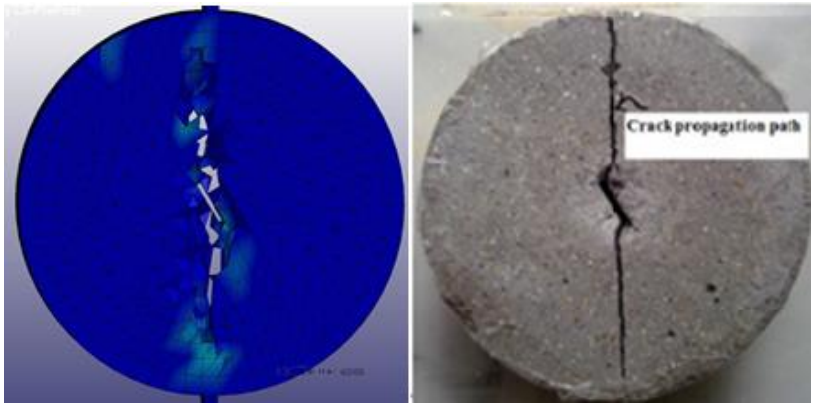

(a) Crack propagation path in EFG result (b) Experiment result [44]

Figure 20: Crack shape when $\varphi = 30^{\circ}$

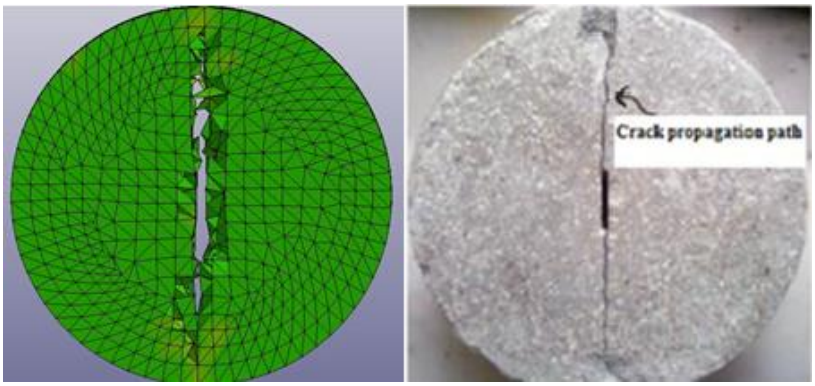

(a) Crack propagation path in EFG result (b) Experiment result [44]

Figure 21: Crack shape when $\varphi = 0^{\circ}$

Conclusion

Four numerical methods are discussed and their capability in LS-DYNA is evaluated. It is concluded that these implementations work well for 3-d crack propagation when proper criterion or algorithm is chosen. DEM, EFG and XFEM show their ability to predict fracture parameters and crack path. However, these three relatively new methods still have their limitations for ease of use and generality to perform fragmentation simulations. For DEM, regularly spaced element arrangement cannot predict crack direction right and cannot capture crack branching. For EFG method, mixed mode crack propagation still needs to be incorporated and its accuracy in predicting stress intensity factors still need to be checked. For XFEM, only 2D analysis is available in LS-DYNA.

Acknowledgement

We would like to thank Ohio Supercomputer Center for the high performance computing resource, without which this research would be impossible.

References

[1] Tabiei A, Wu j. Development of the dyna3d simulation code with automated farcture procedure for brick elements. 7th international LS-DYNA user conferecne 2004.
[2] Aliabadi M. A new generation of boundary element methods in fracture mechanics. Int J Fract 1997;86:91-125.
[3] Petit C, Vergne A, Zhang X. A comparative numerical review of cracked materials. Eng Fract Mech 1996;54:423-39.
[4] Parker A. The mechanics of fracture and fatigue: an introduction. : Spon Press, 1981.
[5] Sih GC. Strain-energy-density factor applied to mixed mode crack problems. Int J Fract 1974;10:305-21.
[6] Gullerud AS, Dodds Jr. RH, Hampton RW, Dawicke DS. Three-dimensional modeling of ductile crack growth in thin sheet metals: computational aspects and validation. Eng Fract Mech 1999;63:347-74.
[7] Wu EM. Application of fracture mechanics to anisotropic plates. Journal of Applied Mechanics 1967;34:967-74.
[8] Irwin G. Relation of stresses near a crack to the crack extension force. 9th Cong.App.Mech., Brussels 1957.
[9] Mi Y. Three-dimensional analysis of crack growth. : Computational mechanics, 1996.
[10] Cundall PA, Strack OD. A discrete numerical model for granular assemblies. Geotechnique 1979;29:47-65.
[11] Jing L, Stephansson O. Fundamentals of Discrete Element Methods for Rock Engineering: Theory and Applications: Theory and Applications. : Elsevier, 2007.
[12] Gullerud AS, Gao X, Dodds Jr RH, Haj-Ali R. Simulation of ductile crack growth using computational cells: numerical aspects. Eng Fract Mech 2000;66:65-92.
[13] Donzé FV, Richefeu V, Magnier S. Advances in discrete element method applied to soil, rock and concrete mechanics. State of the art of geotechnical engineering.Electronic Journal of Geotechnical Engineering 2009;44:31.
[14] Zubelewicz A, Bazant ZP. Interface element modeling of fracture in aggregate composites. J Eng Mech 1987;113:1619-30.
[15] Hedjazi L, Martin CL, Guessasma S, Della Valle G, Dendievel R. Application of the Discrete Element Method to crack propagation and crack branching in a vitreous dense biopolymer material. Int J Solids Structures 2012;49:1893-9.
[16] Masuya H, Kajikawa Y, Nakata Y. Application of the distinct element method to the analysis of the concrete members under impact. Nucl Eng Des 1994;150:367-77.
[17] Brara A, Camborde F, Klepaczko J, Mariotti C. Experimental and numerical study of concrete at high strain rates in tension. Mech Mater 2001;33:33-45.
[18] Tavarez FA, Plesha ME. Discrete element method for modelling solid and particulate materials. Int J Numer Methods Eng 2007;70:379-404.
[19] Gdoutos EE. Strain energy density failure criterion: mixed-mode crack growth. In: Anonymous Fracture Mechanics: Springer; 1993, p. 195-238.

[20] Jensen A, Kirk F, Laird G. Improving the Precision of Discrete Element Simulations through Calibration Models. 13th International LS-DYNA Users Conference 2014.
[21] Belytschko T, Lu YY, Gu L. Element-free Galerkin methods. Int J Numer Methods Eng 1994;37:229-56.
[22] Belytschko T, Krongauz Y, Organ D, Fleming M, Krysl P. Meshless methods: an overview and recent developments. Comput Methods Appl Mech Eng 1996;139:3-47.
[23] Belytschko T, Lu Y, Gu L, Tabbara M. Element-free Galerkin methods for static and dynamic fracture. Int J Solids Structures 1995;32:2547-70.
[24] Belytschko T, Organ D, Krongauz Y. A coupled finite element-element-free Galerkin method. Comput Mech 1995;17:186-95.
[25] Guo Y, Wu C. XFEM and EFG Cohesive Fracture Analysis for Brittle and Semi-Brittle Materials.
[26] Tvergaard V, Hutchinson JW. The influence of plasticity on mixed mode interface toughness. J Mech Phys Solids 1993;41:1119-35.
[27] Abdelaziz Y, Hamouine A. A survey of the extended finite element. Comput Struct 2008;86:1141-51.
[28] Dolbow J, Belytschko T. A finite element method for crack growth without remeshing. Int.J.Numer.Meth.Engng 1999;46:131-50.
[29] Belytschko T. Elastic crack growth in finite elements with minimal remeshing.
[30] Melenk JM, Babuška I. The partition of unity finite element method: basic theory and applications. Comput Methods Appl Mech Eng 1996;139:289-314.
[31] Babuska I, Melenk JM. The partition of unity finite element method 1995.
[32] Osher S, Fedkiw RP. Level set methods: an overview and some recent results. Journal of Computational physics 2001;169:463-502.
[33] Fries T, Belytschko T. The extended/generalized finite element method: an overview of the method and its applications. Int J Numer Methods Eng 2010;84:253-304.
[34] Sukumar N, Moës N, Moran B, Belytschko T. Extended finite element method for three-dimensional crack modelling. Int J Numer Methods Eng 2000;48:1549-70.
[35] Belytschko T, Moës N, Usui S, Parimi C. Arbitrary discontinuities in finite elements. Int J Numer Methods Eng 2001;50:993-1013.
[36] ASTM. ASTM E8: Standard Test Methods for Tension Testing of Metallic Materials. In: Anonymous ; 2012.
[37] Dawicke D, Newman J. Residual strength predictions for multiple site damage cracking using a three-dimensional finite element analysis and a CTOA criterion. Fatigue and fracture mechanics: 29 th 1999:815-29.
[38] Marzougui D. Implementation of a fracture failure model to a 3d non-linear dynamic finite element code (DYNA3D). 1998.
[39] Broek D. Elementary engineering fracture mechanics. : Springer Science & Business Media, 1982.
[40] Tada H, Paris P, Irwin G. The analysis of cracks handbook. : New York: ASME Press, 2000.
[41] Hedjazi L, Guessasma S, Della Valle G, Benseddiq N. How cracks propagate in a vitreous dense biopolymer material. Eng Fract Mech 2011;78:1328-40.
[42] Van de Velde K, Kiekens P. Biopolymers: overview of several properties and consequences on their applications. Polym Test 2002;21:433-42.
[43] Movchan AB, Movchan NV. Mathematical modelling of solids with nonregular boundaries. : CRC Press, 1995.

[44] Haeri H, Shahriar K, FatehiMarji M, Moarefvand P. On the crack propagation analysis of rock like Brazilian disc specimens containing cracks under compressive line loading. Latin American Journal of Solids and Structures 2014;11:1400-16.